

Testing the Cosmic Shear Spatially-Flat Universe Approximation with GLaSS

Peter L. Taylor,* Thomas D. Kitching, and Jason D. McEwen
Mullard Space Science Laboratory, University College London,
Holmbury St. Mary, Dorking, Surrey RH5 6NT, UK

Thomas Tram
Department of Physics and Astronomy, University of Aarhus,
Ny Munkegade 120, DK-8000 Aarhus C, Denmark and
Aarhus Institute of Advanced Studies (AIAS), Aarhus University, DK-8000 Aarhus C, Denmark
(Dated: 12 March 2018)

We introduce the Generalised Lensing and Shear Spectra (GLaSS) code which is available for download from <https://github.com/astro-informatics/GLaSS>. It is a fast and flexible public code, written in Python, that computes generalized spherical cosmic shear spectra. The commonly used tomographic and spherical Bessel lensing spectra come as built-in run-mode options. GLaSS is integrated into the *Cosmosis* modular cosmological pipeline package. We outline several computational choices that accelerate the computation of cosmic shear power spectra. Using GLaSS, we test whether the assumption that using the lensing and projection kernels for a spatially-flat universe – in a universe with a small amount of spatial curvature – negligibly impacts the lensing spectrum. We refer to this assumption as The Spatially-Flat Universe Approximation, that has been implicitly assumed in all cosmic shear studies to date. We confirm that The Spatially-Flat Universe Approximation has a negligible impact on Stage IV cosmic shear experiments provided that a sensible, yet still conservative, bound on Ω_k is adopted.

I. INTRODUCTION

The shape of distant galaxies is distorted by inhomogeneities in the gravitational field along the line of sight; a phenomenon known as gravitational lensing. When the distortion is small, as is most commonly the case, the change in shape is a change in the size and ellipticity of the observed image; known as shear. The gravitational lensing caused by large-scale structure, and in particular the two-point correlation function or power spectrum of this effect, is called cosmic shear.

Experiments that measure cosmic shear are sensitive to the physics of the late Universe, making them an ideal probe to distinguish between models of dark energy [1]. Stage IV weak lensing experiments, that include Euclid¹ [2], WFIRST² [3] and LSST³ [4], will provide an order of magnitude improvement in the precision and accuracy of cosmological parameter estimation over existing surveys [5].

To prepare for these upcoming experiments we must prepare fast and accurate codes to compute the theoretical cosmic shear power spectra for any cosmology. While there are already publicly available tomographic lensing codes that use the Limber approximation [ask Tom for citations], there are no other codes that can compute the cosmic shear power spectra with an arbitrary weight function. It remains an open question which weight-function optimally extracts cosmological information, and we leave this for future work.

Also, before the arrival of Stage IV data, it is vital to test the validity of all assumptions used in cosmic shear studies. One of these approximations is that for the purposes of computing the cosmic shear power spectra we can always treat the Universe as spatially flat. This is an assumption that has not been tested previously.

The structure of this paper is as follows. In Section II we review the equations for the cosmic shear power spectra and the effect of spatial-curvature on the lensing kernel and projection kernel. In Section III we introduce GLaSS, which computes lensing spectra, and discuss a few computational choices that we implemented to speed up the computation of cosmic shear power spectra. Finally in Section IV we demonstrate the speed of GLaSS and discuss the impact of the Spatially-Flat Universe Approximation.

II. FORMALISM

A. Generalized-Spherical Lensing Spectra

The *generalized spherical-transform* is defined by (Taylor et al. 2018):

$$\gamma_{\ell m}(\eta) = \sqrt{\frac{2}{\pi}} \sum_g \gamma_g(r_g, \theta_g) W_\ell(\eta, r_g) {}_2Y_{\ell m}(\theta_g), \quad (1)$$

where $\gamma \in \mathbb{C}$ is the shear, the sum is over all galaxies g with angular coordinate θ_g and radially coordinate r_g , W_ℓ is a weight and ${}_2Y_{\ell m}$ are the spin-2 spherical harmonics. The cosmic shear power spectrum in this

* peterllewelyntaylor@gmail.com

¹ <http://euclid-ec.org>

² <https://www.nasa.gov/wfirst>

³ <https://www.lsst.org>

basis is:

$$C_\ell^{\gamma\gamma}(\eta_1, \eta_2) = \frac{9\Omega_m^2 H_0^4}{16\pi^4 c^4} \frac{(\ell+2)!}{(\ell-2)!} \int \frac{dk}{k^2} G_\ell^\gamma(\eta_1, k) G_\ell^\gamma(\eta_2, k), \quad (2)$$

where Ω_m is the fractional energy density of matter, c is the speed of light in vacuum and H_0 is the value of the Hubble constant today. The G -matrix is:

$$G_\ell^\gamma(\eta, k) \equiv \int dz_p dz' n(z_p) p(z'|z_p) \times W_\ell(\eta, r[z']) U_\ell(r[z'], k) \quad (3)$$

and the U -matrix is:

$$U_\ell(r[z], k) \equiv \int_0^r dr' \frac{F_K(r, r')}{a(r')} j_\ell(kr') P^{1/2}(k; r'), \quad (4)$$

where a is the scale factor, $j_\ell(kr)$ are the spherical Bessel functions and $P(k; r)$ is the power spectrum. The radial distribution of galaxies is denoted by $n(z)$ and $p(z|z')$ gives the probability that a galaxy has a redshift z , given a photometric redshift measurement z' . For a spatially-flat cosmology the lensing kernel, $F_K(r, r')$, is:

$$F_K(r, r') \equiv \frac{r-r'}{rr'}. \quad (5)$$

The power spectrum caused by the random ellipticity component of galaxies, the shot noise spectrum, is given by:

$$N_\ell^{ee}(\eta_1, \eta_2) = \frac{\sigma_e^2}{2\pi^2} \int dz n(z) W_\ell(\eta_1, r) W_\ell(\eta_2, r), \quad (6)$$

where σ_e^2 is the variance of the intrinsic (unlensed) ellipticities of the observed galaxies. We take $\sigma_e = 0.3$ throughout [6].

Taking the weight-function, $W_\ell(\eta, r[z]) \equiv j_\ell(\eta r[z])$ in equations (3) and (6) yields the equations for ‘3D cosmic shear’ first proposed in [7]. To recover the ‘tomographic’ cosmic shear spectra, first proposed in [8], we take the weight function, W^I , as a top hat function in redshift only:

$$W^I(z) \equiv \begin{cases} 1 & \text{if } z \in I \\ 0 & \text{if } z \notin I, \end{cases} \quad (7)$$

the tomographic bin associated with redshift region I .

Taking the Limber approximation [9], the U -matrix becomes:

$$U_\ell(r, k) = \frac{F_k(r, \nu(k))}{ka(\nu(k))} \sqrt{\frac{\pi}{2(\ell+1/2)}} P^{1/2}(k, \nu(k)), \quad (8)$$

where $\nu(k) \equiv \frac{\ell+1/2}{k}$. This is a good approximation for $\ell > 100$ [10].

B. The Lensing Kernel for $\Omega_k \neq 0$

In a spatially-curved universe, the expression for the lensing kernel in equation (5) must be replaced by the more general expression:

$$F_K(r, r') \equiv \frac{f_k(r-r')}{f_k(r)f_k(r')}, \quad (9)$$

where $f_k(r)$ is the co-moving angular distance [11]. This is given by:

$$f_K(r) \equiv \begin{cases} K^{-1/2} \sin(K^{1/2}r) & \text{if } K > 0 \\ r & \text{if } K = 0. \\ (-K)^{-1/2} \sinh((-K)^{1/2}r) & \text{if } K < 0. \end{cases} \quad (10)$$

where the curvature, K , is defined as $K \equiv -(H_0/c^2)\Omega_k$, and Ω_k is the fractional dimensionless energy density of curvature in the Universe.

C. The Projection Kernel for $\Omega_k \neq 0$

In a spatially-flat universe, the gravitational potential at a time labeled by the redshift z , $\Phi(\mathbf{r}; z)$, is related to the underlying density field, $\delta(\mathbf{r}; z)$, by the Poisson equation:

$$\nabla_r^2 \Phi(\mathbf{r}; z) = \frac{3\Omega_m H_0^2}{2a(t)} \delta(\mathbf{r}; z), \quad (11)$$

where ∇_r^2 is the Laplacian associated with a spatially-flat universe.

The potential, $\Phi(\mathbf{r}; z)$, in the observer’s frame is given in a coordinate system defined by two angles on the sky and a radial distance denoted by (r, θ, ϕ) . Meanwhile the density field is in rectilinear coordinates. To relate the two, and hence find the lensing spectra in terms of the matter power spectrum, we expand the potential in spherical Bessel space:

$$\Phi_{\ell m}(\mathbf{r}) = \sqrt{\frac{2}{\pi}} \int d^3r \Phi(r) j_\ell(kr) Y_{\ell m}(\theta, \phi), \quad (12)$$

where $j_\ell(kr)$ are spherical Bessel functions and $Y_{\ell m}(\theta, \phi)$ are spherical harmonics. Then since spherical harmonics and spherical Bessel functions are eigenfunctions of the Laplace operator, we have:

$$(\nabla_r^2 + k^2) j_\ell(kr) Y_{\ell m}(\theta, \phi) = 0, \quad (13)$$

and from equation (11) the lensing potential is related to the density field in harmonic space by:

$$\Phi_{\ell m}(\mathbf{r}; z) = -\frac{3\Omega_m H_0^2}{2k^2 a(t)} \delta_{\ell m}(\mathbf{r}; z). \quad (14)$$

From this it is possible to derive the expression for the cosmic shear power spectrum. Since Bessel functions

relate the lensing potential in rectilinear coordinates to a projected shear signal on the sky, we refer to $j_\ell(kr)$ as the *projection kernel*. In the final expression for the cosmic shear power spectra, the projection kernel is found in the U -matrix (see [12] for a full derivation).

Meanwhile in a spatially-curved universe, we must take the Laplacian associated with the curved Robertson-Walker metric [13] in equation (11). Hence the projection kernel must change too. In particular spherical Bessel functions must be replaced by hyperspherical Bessel functions, $\Phi_\ell^\beta(r)$, because they are eigenfunctions of the the Laplace operator in a spatially-curved cosmology. That is:

$$\left(\nabla_{S_K(\chi)}^2 + (ck)^2\right) \Phi_\ell^\beta(\chi) Y_{\ell m}(\theta, \phi) = 0, \quad (15)$$

where $\beta \equiv \sqrt{(ck)^2 + K}$, $\chi = r/c$ and

$$S_K(\chi) \equiv \begin{cases} \sin \chi & \text{if } K > 0 \\ \chi & \text{if } K = 0 \\ \sinh \chi & \text{if } K < 0. \end{cases} \quad (16)$$

Following the same argument used in the spatially-flat case, we find the hyperspherical Bessel functions enter the U -matrix, in place of the normal spherical Bessel functions, as the projection kernel.

The Limber approximation also has to be generalized to spatially-curved cosmologies [14]. In this case the Limber-approximated U -matrix becomes:

$$U_\ell(r, k) = \left(1 - \hat{K} \frac{\ell^2}{\beta^2}\right)^{-\frac{1}{4}} U_\ell^{\text{flat}}(r, k), \quad (17)$$

where \hat{K} is the sign of the curvature K , and $U_\ell^{\text{flat}}(r, k)$ is the Limber approximated U -matrix for a spatially-flat universe defined in equation (8).

III. THE GLASS CODE

We now describe the GLaSS code that can compute all the power spectra previously described.

A. Description and Run Options

GLaSS is a flexible code written in Python and it is fully integrated into the `Cosmosis` modular cosmological pipeline [15]. The code is provided with Python wrappers and cosmological information can be read directly from the `Cosmosis` pipeline or from an external source.

There are numerous run-mode options. The user can choose between several weights. These include: the top hats associated with tomographic binning with an equal number of galaxies per bin or equally spaced tomographic bins in redshift, the spherical Bessel weight,

or a customized weight provided by the user. The number of tomographic bins can also be varied. The user can specify which ℓ -modes to sample over a prescribed redshift range. The package is distributed with default functional forms for the radial distribution of galaxies, $n(z)$, and photometric redshift error $p(z|z')$. These are:

$$p(z|z_p) \equiv \frac{1}{2\pi\sigma_z(z_p)} e^{-\frac{(z-c_{\text{cal}}z_p+z_{\text{bias}})^2}{2\sigma_{z_p}^2}}, \quad (18)$$

with $c_{\text{cal}} = 1$, $z_{\text{bias}} = 0$ and $\sigma_{z_p} = A(1+z_p)$, with default value is $A = 0.05$ [16] and

$$n(z_p) \propto \frac{a_1}{c_1} e^{-\frac{(z-0.7)^2}{b_1^2}} + e^{-\frac{(z-1.2)^2}{d_1^2}}, \quad (19)$$

with default values $(a_1/c_1, b_1, d_1) = (1.5/0.2, 0.32, 0.46)$ [17]. It is possible for the user to provide custom functional forms too.

The Limber approximation can be turned on or off. Since the Limber approximation is less accurate at low- ℓ [10], it can be turned on for any chosen $\ell > \ell_{\text{Lim}}$, for a specified value of ℓ_{Lim} .

Finally it is possible to independently turn the spatially-curved lensing kernel and projection kernel approximations on or off; however later we show these approximations have negligible impact. Hyperspherical Bessel functions are computed with a Python wrapper that calls CLASS [18]. Details about the implementation of the hyperspherical Bessel functions in CLASS are given in ([19] and [14]).

GLaSS has been compared to the spherical Bessel code used in [20] and gives very similar output when using the spherical Bessel weight (Spurio Mancini et al. in prep).

B. Computational Choices

Several numerical choices have been implemented in GLaSS to reduce the computation time.

Values of the Bessel functions, $j_\ell(x)$, are computed just once and stored in a 2D look up table in ℓ and x . The values of $j_\ell(kr)$, can then found as needed. We sample sufficiently densely in x so that final lensing spectra is not affected above machine precision. Compressing the data in this way reduces memory requirements and was used before in [13, 21]. In the hyperspherical case, it is not possible to compress the data to a 2D-array. In this case the hyperspherical Bessel functions are computed on the fly, slowing down the total computation time.

Even though the Bessel functions need only be computed once, the computation of these has also been optimized in GLaSS. For a given argument x , GLaSS computes and stores all $j_\ell(x)$ for all ℓ -modes simultaneously using Miller's algorithm which is based on recurrence relations and implemented in the `GNU Scientific`

Library [22], and called using `ctypesGSL`. If the maximum ℓ is too high, Miller’s algorithm suffers from underflow. `GLaSS` avoids this by first sparsely sampling the x -range to determine a maximum $\ell_{\max}(x)$, for each x , which is defined as the ℓ -value past which the Bessel functions fall below machine precision. `GLaSS` sets $j_\ell(x) = 0$ for all $\ell > \ell_{\max}(x)$.

As the Bessel functions are pre-computed, the majority of the computation time is taken by evaluating the nested integrals in equations (1) - (4). In `GLaSS` all these are evaluated using matrix multiplications on a grid in r and k . For example the U -matrix can be written as a matrix multiplication given by:

$$U_\ell(r, k) \approx \sum_{r'} A(r, r') B(r', k), \quad (20)$$

$A(r, r') \equiv \Delta r' \frac{F_K(r, r')}{a(r')}$, where $\Delta r'$ is the spacing the spacing of the grid in r' and $B(r, r') \equiv j_\ell(kr') P^{1/2}(k; r')$.

All matrix multiplications in `GLaSS` are implemented using the `numpy.dot` function. This is one of the few functions that releases the Global Interpreter Lock in `Python`, so the matrix multiplications are parallelized when `numpy` is linked to a linear algebra library such as BLAS (Basic Linear Algebra Subprograms), Math Kernel Library (MKL) or Apple Accelerate. There are also MPI run-mode options for the Monte Carlo samplers in `Cosmosis`, which can be used to further distribute the workload over multiple cores.

The final speed improvements comes from making the Limber approximation. Since the Bessel functions oscillate quickly, particularly for high- ℓ , making the Limber approximation reduces the size of the computation grid needed to accurately evaluate the U -matrix. Meanwhile `GLaSS` can simultaneously turn the Limber approximation off at low- ℓ so that accuracy is not lost at these large angular scales where the Limber approximation is invalid.

IV. RESULTS

We now present results on the `GLaSS` computational scaling, and the impact of the spatially-flat universe approximation.

A. GLaSS Module Timing

We now present the results of several speed tests using `GLaSS`. All results cited are for 10-bin tomography with an equal number of galaxies per bin sampling 50 ℓ -modes below $\ell_{\max} = 3000$ on a single 2.7 GHz Intel i5 Core on a 2015 Macbook Pro with 8 GB of RAM.

It takes 28 seconds to compute all the Bessel function data, but this must only ever be computed once. This shows how vital it is to pre-compute the Bessel data.

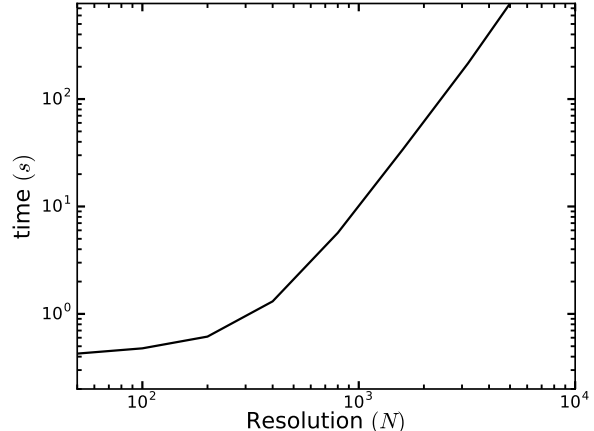


FIG. 1. Time to compute 50 ℓ -modes in `GLaSS` against grid resolution N (i.e. number of tomographic bins, or k -modes in 3D cosmic shear) on a single 2.7 GHz Intel i5 Core. Spectra for resolutions up to $N = 400$ can all be computed in less than 1.5s. This is a sufficient resolution to evaluate the tomographic cosmic shear power spectra and recover all information from the 3D shear field (Taylor et al. 2018). At high- ℓ , the computation time, t , is dominated by the matrix multiplications and hence scales as $t \propto N^{2.87}$.

The lensing spectra are computed on an $N \times N$ grid, where N are the number of tomographic bins, where the diagonal part are the auto-correlation power spectra and the off-diagonal are the cross-correlation power spectra. A plot of the computation time versus the grid resolution, N , is shown in Figure 1. The Limber approximation is assumed for $\ell > 100$. For $N < 300$, it takes less than a second to compute the lensing spectra.

As the resolution is increased beyond $N = 600$, the computation time, t , follows the power law $t \propto N^{2.87}$. This reflects the fact that the computation time becomes dominated by the nested matrix multiplications. Naively matrix multiplications scale as $\mathcal{O}(N^3)$ because all N^2 elements of the first matrix must be multiplied by N elements in the second matrix. Our code does slightly better and scales as $\mathcal{O}(N^{2.87})$ because it uses the highly optimized `numpy.dot` routine.

It was shown in (Taylor et al. 2018) that a resolution of $N = 400$ is sufficient to capture nearly all the lensing kernel and power spectrum information. Meanwhile a resolution of $N = 2000$ is required to capture 80% of the information when using the spherical Bessel weight and an extremely high resolution of $N = 5000$ is needed to capture 97% of the information for this choice of weight (Taylor et al. 2018).

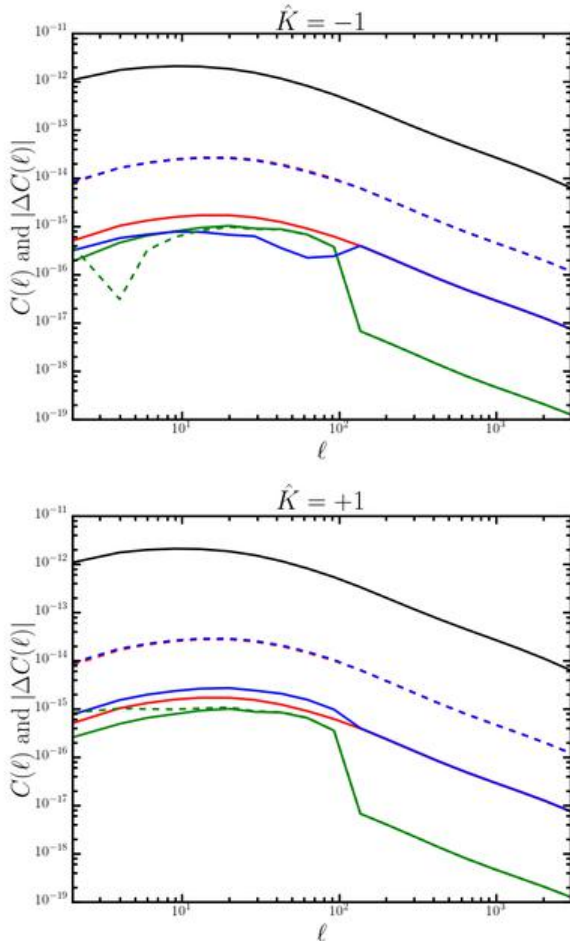


FIG. 2. The cross-correlated lensing power spectrum between the 9th and 10th tomographic bins. 10-bin tomography with an equal number of galaxies per bin, is used. The Limber approximation is taken for $\ell > 100$. **Black:** The fiducial cosmic shear power spectrum using the spatially-flat lensing kernel and spatially-flat Bessel functions. The **coloured lines** show the absolute value of the difference between the fiducial power spectra and different combinations of the spatially-curved lensing kernel and hyperspherical approximations turned on and off. **Dashed lines** are for $|\Omega_k| = 0.08$; this is the expected 1σ constraint on Ω_k from Stage IV cosmic shear experiments alone. **Solid lines** are for $|\Omega_k| = 0.005$; this is the Planck Prior. **Red:** Spatially-curved lensing kernel and spatially-flat Bessel functions. **Green:** Spatially-flat lensing kernel and spatially-curved Bessel functions. **Blue:** Spatially-curved lensing kernel and spatially-curved Bessel functions.

B. Impact of the Flat Universe Approximation on Lensing Spectra

We compute the cosmic shear power spectra with all combinations of the spatially-flat Bessel function approximation and spatially-flat lensing kernel approximation turned on or off. The Limber approximation is used for $\ell > 100$ and we use the spatially-curved gen-

eralization when the spatially-curved lensing kernel is turned on. Ten bin tomography with an equal number of galaxies per bin is used over a 15,000 degree survey with 30 galaxies per square arcminute mimicking the Euclid wide-field survey. We take the lensing spectrum generated using spatially-flat lensing and projection kernels, as the fiducial model since all studies to date have used this approximation.

All spectra are computed using the same flat fiducial cosmology with: $(\Omega_m, \Omega_k, \Omega_b, h_0, n_s, A_s, \tau) = (0.315, 0.0, 0.04, 0.67, 0.96, 2.1 \times 10^9, 0.08)$. The linear power spectrum is generated using CAMB [23] and the non-linear part is generated using HALOFIT [24].

The cross-correlated lensing power spectrum between the two largest tomographic bins is shown in Figure 2. These bins were chosen because the effects of spatial curvature are maximal in the highest redshift bins and the signal-to-noise in the auto-correlation of the highest redshift bin is relatively small due to shot noise, whereas the cross-correlation is noise-free. The absolute value of the difference between the fiducial spectrum and spectra with various combinations of the spatially-flat lensing kernel and spatially-flat Bessel functions turned on or off are shown in the colored lines. The dashed lines are for $\Omega_k = 0.08$. This is the expected 1σ constraints on Ω_k from a Euclid-like experiment [25]. The solid lines are used for $|\Omega_k| = 0.005$. This is the Planck 2σ prior on $|\Omega_k|$ [26]. Both are extremely conservative overestimates of constraints on curvature as multi-probe constraints place $100 |\Omega_k| < 0.7$ [27].

For the $|\Omega_k| = 0.005$ case the impact of changing the lensing and projection kernels is negligible. The lensing spectrum is impacted by less than 0.2%. This is similar to the impact of the Limber approximation at $\ell = 1000$ [10]. There is a bump in the solid green line that gives the difference between the fiducial spectrum and the spectrum with the curved-sky projection kernel and the flat-sky lensing kernel. This is because we take the Limber approximation and its spatially-curved equivalent above $\ell = 100$. The relative 1% bump in the green line at $\ell = 100$ is consistent with the error due to the Limber Approximation at this ℓ -mode [10], that we see in this plot since the error is caused by the spatially-flat approximation is similarly small.

For the $|\Omega_k| = 0.08$ case changing the projection kernel has an extremely similar impact as in the $|\Omega_k| = 0.005$ case, that is the dashed and solid green lines are very similar. This is expected since the magnitude of $|K|$ only impacts the projection kernel from the definition of $\beta = \sqrt{(ck)^2 + K}$ used in the hyperspherical Bessel function $\Phi_\ell^\beta(r)$. The curvature, K , is negligible in this expression except when k is small. Lensing is sensitive to these small- k modes in the power spectrum at small ℓ (Taylor et al. 2018). This is precisely where there is a difference between the $|\Omega_k| = 0.08$ and the $|\Omega_k| = 0.005$ case.

Using the spatially-curved lensing kernel in the $|\Omega_k| = 0.08$ case has a larger impact; the difference is indicated by the dashed blue lines. Above $\ell = 100$ changing the

lensing kernel results in a 1% change from the fiducial case, but never more than 2%. This is similar to the change in power due to the Limber approximation [10] at $\ell = 100$. However changing the lensing kernel impacts all ℓ -modes. Thus, to avoid any risk of bias in a future survey we recommend either enforcing the conservative Planck bound: $|\Omega_k| < 0.005$, or using the full spatially-curved lensing kernel. This comes at little additional computational cost since we showed in the previous section that the lensing computation time is dominated by integration.

V. CONCLUSION

We have presented the GLaSS code that computes generalized cosmic shear power spectra. Spherical Bessel and tomographic lensing spectra with an equal number of galaxies per bin and equal redshift run-mode options are available. More generally GLaSS is capable of computing the lensing spectra with *any* data weighting. This should prove useful for determining the optimal weight for shear data in upcoming surveys.

GLaSS is fast. Using the Limber approximation, GLaSS can compute a 10-bin tomographic lensing spec-

tra for a single cosmology, sampling 50 ℓ -modes, in less than 0.4s. For Stage IV experiments where the Limber approximation must be dropped below $\ell < 100$, the same spectra is computed in 1.3s.

Using GLaSS we have tested the Spatially-Flat Universe Approximation, which is implicitly assumed in all cosmic shear studies to date. We find this is an accurate approximation and it is unnecessary to compute the full expression for upcoming surveys provided a conservative bound of $|\Omega_k| < 0.005$ is enforced. For cosmic shear surveys that do not impose any external bound on Ω_k , we recommend using the full spatially-curved lensing kernel. This comes at little additional computational cost and ensures that spatial-curvature will only bias the lensing spectra by $< 0.1\%$ from the projection kernel. It is therefore not necessary to account for the effects of spatial curvature on the projection kernel.

ACKNOWLEDGEMENTS

We thank the *Cosmosis* team for making their code publicly available. PT is supported by the UK Science and Technology Facilities Council. TK is supported by a Royal Society University Research Fellowship. The authors acknowledge the support of the Leverhulme Trust.

-
- [1] A. Refregier, A. Amara, T. Kitching, A. Rassat, R. Scaramella, J. Weller, *et al.*, arXiv preprint arXiv:1001.0061 (2010).
 - [2] R. J. Laureijs, L. Duvet, I. E. Sanz, P. Gondoin, D. H. Lumb, T. Oosterbroek, and G. S. Criado, in *Proc. SPIE*, Vol. 7731 (2010) p. 77311H.
 - [3] D. Spergel, N. Gehrels, C. Baltay, D. Bennett, J. Breckinridge, M. Donahue, A. Dressler, B. Gaudi, T. Greene, O. Guyon, *et al.*, arXiv preprint arXiv:1503.03757 (2015).
 - [4] J. Anthony and L. Collaboration, in *Proc. of SPIE Vol.*, Vol. 4836, p. 11.
 - [5] A. Albrecht, G. Bernstein, R. Cahn, W. L. Freedman, J. Hewitt, W. Hu, J. Huth, M. Kamionkowski, E. W. Kolb, L. Knox, *et al.*, arXiv preprint astro-ph/0609591 (2006).
 - [6] M. L. Brown, A. N. Taylor, D. J. Bacon, M. E. Gray, S. Dye, K. Meisenheimer, and C. Wolf, *Monthly Notices of the Royal Astronomical Society* **341**, 100 (2003).
 - [7] A. Heavens, *Monthly Notices of the Royal Astronomical Society* **343**, 1327 (2003).
 - [8] W. Hu, *The Astrophysical Journal Letters* **522**, L21 (1999).
 - [9] M. LoVerde and N. Afshordi, *Physical Review D* **78**, 123506 (2008).
 - [10] T. D. Kitching, J. Alsing, A. F. Heavens, R. Jimenez, J. D. McEwen, and L. Verde, arXiv preprint arXiv:1611.04954 (2016).
 - [11] M. Kilbinger, *Reports on Progress in Physics* **78**, 086901 (2015).
 - [12] P. Castro, A. Heavens, and T. Kitching, *Physical Review D* **72**, 023516 (2005).
 - [13] A. Kosowsky, arXiv preprint astro-ph/9805173 (1998).
 - [14] J. Lesgourgues and T. Tram, *Journal of Cosmology and Astroparticle Physics* **2014**, 032 (2014).
 - [15] J. Zuntz, M. Paterno, E. Jennings, D. Rudd, A. Manzotti, S. Dodelson, S. Bridle, S. Sehrish, and J. Kowalkowski, *Astronomy and Computing* **12**, 45 (2015).
 - [16] O. Ilbert, S. Arnouts, H. McCracken, M. Bolzonella, E. Bertin, O. Le Fevre, Y. Mellier, G. Zamorani, R. Pello, A. Iovino, *et al.*, *Astronomy & Astrophysics* **457**, 841 (2006).
 - [17] L. Van Waerbeke, J. Benjamin, T. Erben, C. Heymans, H. Hildebrandt, H. Hoekstra, T. D. Kitching, Y. Mellier, L. Miller, J. Coupon, *et al.*, *Monthly Notices of the Royal Astronomical Society* **433**, 3373 (2013).
 - [18] D. Blas, J. Lesgourgues, and T. Tram, *Journal of Cosmology and Astroparticle Physics* **2011**, 034 (2011).
 - [19] T. Tram, *Communications in Computational Physics* **22**, 852 (2017).
 - [20] A. Spurio Mancini, R. Reischke, V. Pettorino, B. M. Schaefer, and M. Zumalacárregui, arXiv preprint arXiv:1801.04251 (2018).
 - [21] U. Seljak and M. Zaldarriaga, *ApJ* **469**, 437.
 - [22] B. Gough, *GNU scientific library reference manual* (Network Theory Ltd., 2009).
 - [23] A. Lewis and A. Challinor, *Astrophysics Source Code Library* (2011).
 - [24] R. Takahashi, M. Sato, T. Nishimichi, A. Taruya, and M. Oguri, *The Astrophysical Journal* **761**, 152 (2012).
 - [25] A. Heavens, T. D. Kitching, and A. Taylor, *Monthly Notices of the Royal Astronomical Society* **373**, 105 (2006).

- [26] P. Ade, N. Aghanim, M. Arnaud, M. Ashdown, J. Aumont, C. Baccigalupi, A. Banday, R. Barreiro, J. Bartlett, N. Bartolo, *et al.*, *Astronomy & Astrophysics* **594**, A13 (2016).
- [27] P. A. Ade, N. Aghanim, C. Armitage-Caplan, M. Arnaud, M. Ashdown, F. Atrio-Barandela, J. Aumont, C. Baccigalupi, A. J. Banday, R. Barreiro, *et al.*, *Astronomy & Astrophysics* **571**, A16 (2014).